

Cite this: DOI: 10.1039/c0xx00000x

www.rsc.org/xxxxxx

SUPPORTING INFORMATION

Strong localized surface plasmon resonance effects of Ag/TiO₂ core-shell nanowire arrays in visible light for photocatalytic activity

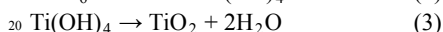
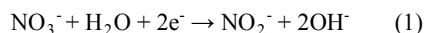
Hyeonjin Eom,^{a,b} Joo-Yun Jung,^b Yosep Shin,^b Sarah Kim,^b Jun-Hyuk Choi,^b Eungsug Lee,^b Jun-Ho Jeong,^{*b} and Inkyu Park^{*a,c}

Received (in XXX, XXX) Xth XXXXXXXXXX 20XX, Accepted Xth XXXXXXXXXX 20XX

DOI: 10.1039/b000000x

Deposition of TiO₂ thin film:

The TiO₂ thin film was deposited by widely used cathodic electrodeposition in aqueous electrolyte¹ that contains 0.1M NH₄NO₃ and 0.05M (NH₄)₂TiF₆.² Some studies on the mechanism of TiO₂ cathodic deposition in (NH₄)₂TiF₆ aqueous solution explain that NO₃⁻ reduction works as the oxidant for Ti(IV) formation³ and significantly affects the formation of TiO₂ film.⁴ The electrodeposition of TiO₂ thin film via the reduction of NO₃⁻ to NO₂⁻ can be described as the following:²



The reduction of NO₃⁻ and accumulation of OH⁻ facilitates the TiO₂ formation on the electrode by the combination of OH⁻ and Ti(IV) species. More details of TiO₂ cathodic electrodeposition can be found in the literature.⁵ Electrodeposition was performed at -1.1V (vs. Ag/AgCl reference electrode) as an optimal potential for reasonably high deposition rate while suppressing the evolution of hydrogen and nitrogen. Current-time (I-t) curve of TiO₂ film electrodeposition is represented on inset of Fig. S1a. The current was stabilized at ~0.4mA after 80sec. Gel-phase TiO₂ film was also fabricated by sol-gel spin coating method. The solution consisted of titanium isopropoxide (Ti(OC₃H₇)₄) as the source for formation of gel TiO₂ film.⁶ After deposition process, films were annealed at 80°C for 30 min to remove the contaminant. The surface morphology of Ag/gel TiO₂ films by electrodeposition process is shown on Fig. S1a and gel-TiO₂ by sol-gel spin coating method is shown on Fig. S1b. The thickness of both gel-TiO₂ films which are fabricated by electrodeposition and sol-gel spin coating methods were measured as ~50nm by spectroscopic ellipsometer (Woollam, M2000D)).

XRD analysis of TiO₂ layer:

For the X-ray diffraction (XRD) analysis of TiO₂ thin film, the films with thickness over 200 nm were deposited due to the detection limit of the XRD equipment. Fig.S2a shows the XRD pattern of the TiO₂ thin film that was electrodeposited on Si (100) substrate with thermally evaporated Ag thin film and thermally annealed at 300 °C for the formation of anatase-phase TiO₂. First, diffraction peaks of Ag and shoulder at low angle

range are observed. Also, the peaks for anatase phase ((101) and (200)) can be observed. The peaks of silver oxide (AgO) are not observed from the XRD data.

XPS analysis of Ag NW and Ag/TiO₂ core-shell NW arrays:

The full range XPS survey spectra of A0 NW, A0/gel NW and A0/anatase NW samples are shown in Fig.S2b. The XPS results of Ti 2p binding energies for as-deposited A0/gel NW and A0/anatase NW are shown in Fig.S2c. The peak position of the Ti(2p_{3/2}) shifted from 459.4 eV to 458.1 eV by the transformation of A0/gel NW to A0/anatase NW. The higher binding energy of A0/gel NW samples was caused by fluorine (F) intermediate on the surface because of the incomplete reaction.^{2, 7} The peak of F in A0/gel NW at 687eV represents the substitutional F atom on oxygen site in the TiO₂ (Fig.S2b)⁸. After annealing, gel film was changed to anatase film (Fig.S2a) and F was removed as shown in Fig.S2b. The peaks of Ti 2p binding energies of Ag/anatase NW at 458.1eV were in accord with anatase-phase TiO₂ in the literature.^{9, 10}

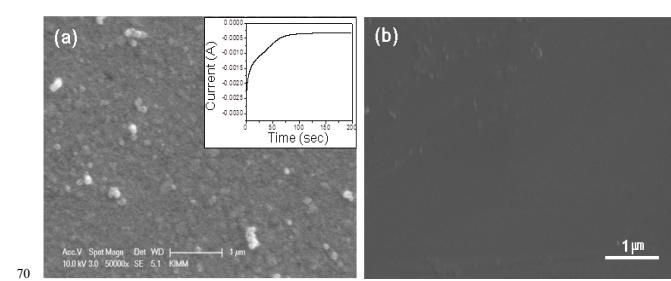


Fig. S1. SEM images of Ag/gel-TiO₂ dual layer film (inset: i-t curve during TiO₂ electrodeposition process on Ag film) and (b) gel-TiO₂ single layer film.

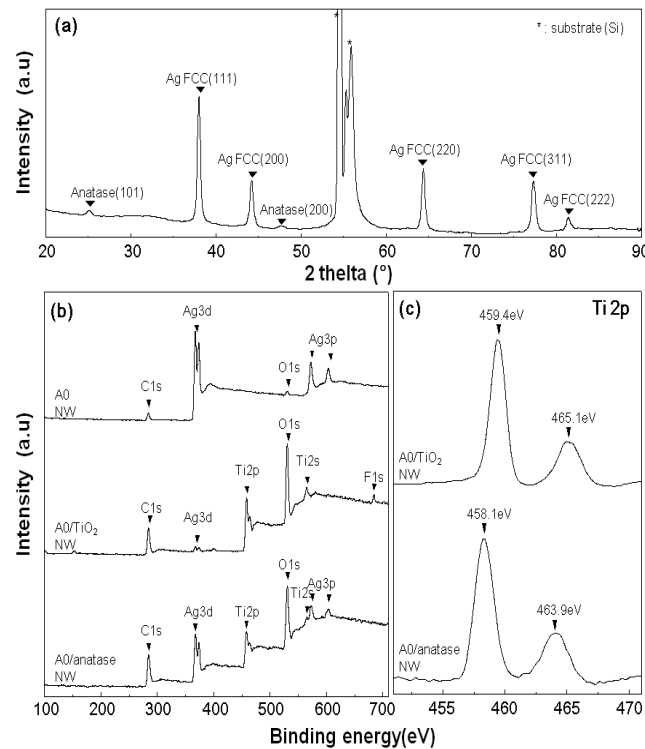


Fig.S2. Surface characterization of fabricated samples: (a) X-ray diffraction pattern of Ag/electrodeposited-TiO₂ dual layer film heated at 300°C. b) XPS spectra of A0 NW, A0/TiO₂ NW and A0/anatase NW, and c) Ti 2p of A0/TiO₂ NW array and A0/anatase NW array.

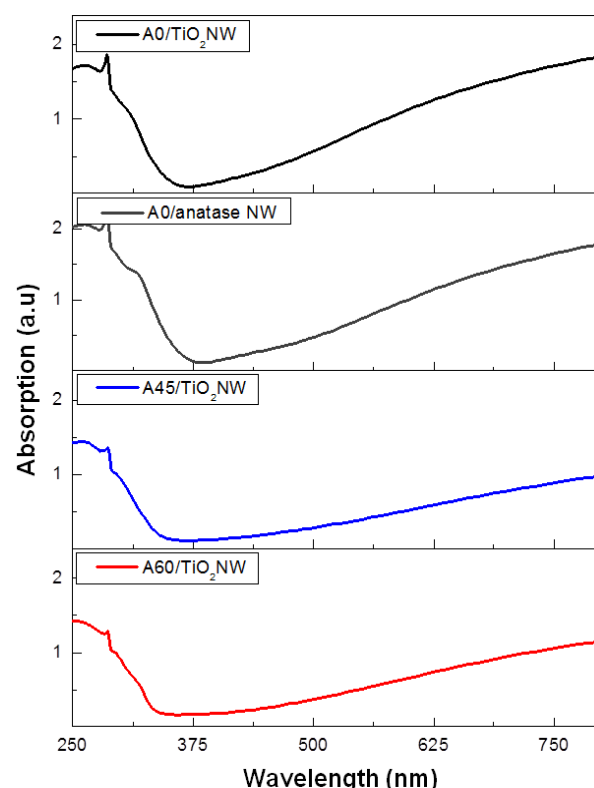


Fig.S4. The simulated transverse electric (TE) mode absorption of (a) A0/TiO₂ NW array, (b) A0/anatase NW array, (c) A45/TiO₂ NW and (d) A60/TiO₂ NW

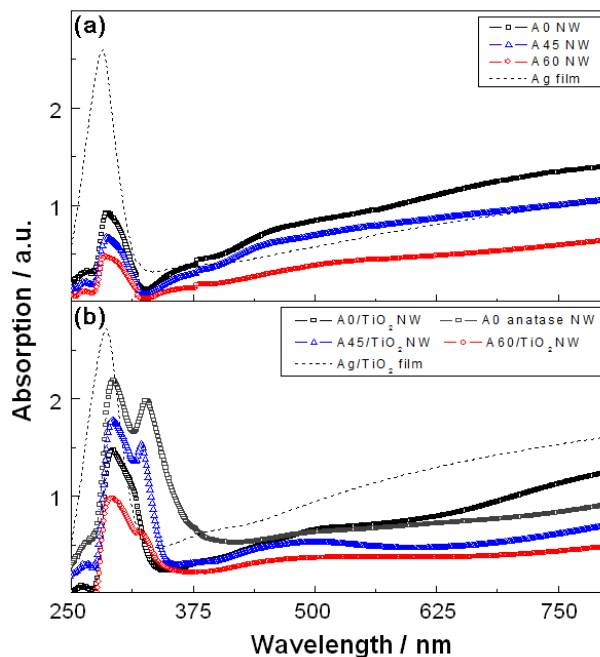


Fig. S3. Measured absorption for transverse electric (TE) mode of (a) A0 NW array, A45 NW array, A60 NW array (b) A0/TiO₂ NW array, A0/anatase NW array, A45/TiO₂ NW array and A60/TiO₂ NW array; Black dotted lines for each sub-figure represent non-polarized absorption of a) Ag thin film and b) Ag/gel-TiO₂ dual layer thin film, respectively.

20 FDTD Numerical Simulation:

The calculations of light absorption were performed by using commercially available 2D finite difference time domain (FDTD) software (Lumerical®, Lumerical Solutions, Inc.). The geometrical parameters for modeling were obtained from the 25 SEM images of the fabricated samples. The structures were illuminated by a linearly polarized broadband incident plane wave. An infinite 2D array of unit cells was simulated using periodic boundary conditions at the left and right boundaries, while perfectly matched layer (PML) absorbing boundary 30 conditions were set at the top and bottom boundaries. The size of mesh cell in the calculations was set as 1 × 1 nm. The 35 Lumerical's multi-coefficient model was used to fit the empirical dielectric constants of Ag, which were taken from Palik's Handbook of Optical Constants.¹¹ The dielectric constants of electrodeposited TiO₂ and anatase TiO₂ were measured by using a Spectroscopic Ellipsometer (M2000D, Woollam) and used in simulation. Measured refractive index (n) and extinction coefficient (k) of gel and anatase TiO₂ are presented on Fig.S5.

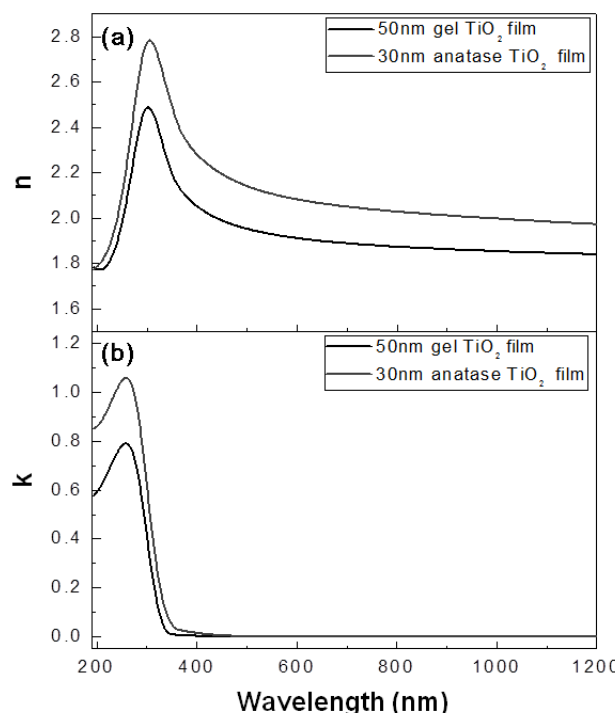


Fig. S5. Optical properties of the gel phase TiO_2 film and anatase TiO_2 film: (a) Refractive index (n) and (b) extinction coefficient (k)

5

References

1. C. Natarajan and G. Nogami, *J Electrochem Soc*, 1996, **143**, 1547-1550.
2. M. Chigane, M. Watanabe, M. Izaki, I. Yamaguchi and T. Shinagawa, *Electrochemical and Solid State Letters*, 2009, **12**, E5-E8.
3. C. C. Hu, H. C. Hsu and K. H. Chang, *J Electrochem Soc*, 2012, **159**, D418-D424.
4. C. C. Huang, H. C. Hsu, C. C. Hu, K. H. Chang and Y. F. Lee, *Electrochimica Acta*, 2010, **55**, 7028-7035.
5. P. M. Dziewonski and M. Grzeszczuk, *Electrochimica Acta*, 2009, **54**, 4045-4055.
6. K. Narasimha Rao, M. Vishwas, S. Kumar Sharma and K. V. Arjuna Gowda, *Proc. of SPIE*, 2008, **7067**, 70670F-70670F-70678.
7. H. M. Yang and X. C. Zhang, *J Mater Chem*, 2009, **19**, 6907-6914.
8. J. C. Yu, J. G. Yu, W. K. Ho, Z. T. Jiang and L. Z. Zhang, *Chem Mater*, 2002, **14**, 3808-3816.
9. K. J. A. Raj, R. Shanmugam, R. Mahalakshmi and B. Viswanathan, *Indian J Chem A*, 2010, **49**, 9-17.
10. K. J. A. Raj, T. Elangovan and B. Viswanathan, *Indian J Chem A*, 2012, **51**, 676-680.
11. Z. K. Zheng, B. B. Huang, X. Y. Qin, X. Y. Zhang, Y. Dai and M. H. Whangbo, *J Mater Chem*, 2011, **21**, 9079-9087.

30